



## The Influence of $\gamma$ - and $\gamma$ -Al<sub>2</sub>O<sub>3</sub> Phases on the Thermoelectric Properties of Al-doped ZnO

Han, Li; Van Nong, Ngo; Le, Thanh Hung; Holgate, Tim; Pryds, Nini; Ohtaki, Michitaka ; Linderorth, Søren

*Published in:*  
Journal of Alloys and Compounds

*Link to article, DOI:*  
[10.1016/j.jallcom.2012.12.091](https://doi.org/10.1016/j.jallcom.2012.12.091)

*Publication date:*  
2013

[Link back to DTU Orbit](#)

*Citation (APA):*  
Han, L., Van Nong, N., Le, T. H., Holgate, T., Pryds, N., Ohtaki, M., & Linderorth, S. (2013). The Influence of  $\gamma$ - and  $\gamma$ -Al<sub>2</sub>O<sub>3</sub> Phases on the Thermoelectric Properties of Al-doped ZnO. *Journal of Alloys and Compounds*, 555, 291–296. <https://doi.org/10.1016/j.jallcom.2012.12.091>

---

### General rights

Copyright and moral rights for the publications made accessible in the public portal are retained by the authors and/or other copyright owners and it is a condition of accessing publications that users recognise and abide by the legal requirements associated with these rights.

- Users may download and print one copy of any publication from the public portal for the purpose of private study or research.
- You may not further distribute the material or use it for any profit-making activity or commercial gain
- You may freely distribute the URL identifying the publication in the public portal

If you believe that this document breaches copyright please contact us providing details, and we will remove access to the work immediately and investigate your claim.

## Accepted Manuscript

The Influence of  $\alpha$ - and  $\gamma$ -Al<sub>2</sub>O<sub>3</sub> Phases on the Thermoelectric Properties of Al-doped ZnO

Li Han, Ngo Van Nong, Le Thanh Hung, Tim Holgate, Nini Pryds, Michitaka Ohtaki, Søren Linderorth

PII: S0925-8388(12)02315-8

DOI: <http://dx.doi.org/10.1016/j.jallcom.2012.12.091>

Reference: JALCOM 27531



To appear in:

Received Date: 7 November 2012

Revised Date: 17 December 2012

Accepted Date: 18 December 2012

Please cite this article as: L. Han, N.V. Nong, L.T. Hung, T. Holgate, N. Pryds, M. Ohtaki, S. Linderorth, The Influence of  $\alpha$ - and  $\gamma$ -Al<sub>2</sub>O<sub>3</sub> Phases on the Thermoelectric Properties of Al-doped ZnO, (2012), doi: <http://dx.doi.org/10.1016/j.jallcom.2012.12.091>

This is a PDF file of an unedited manuscript that has been accepted for publication. As a service to our customers we are providing this early version of the manuscript. The manuscript will undergo copyediting, typesetting, and review of the resulting proof before it is published in its final form. Please note that during the production process errors may be discovered which could affect the content, and all legal disclaimers that apply to the journal pertain.

# 1 The Influence of $\alpha$ - and $\gamma$ -Al<sub>2</sub>O<sub>3</sub> Phases on the 2 Thermoelectric Properties of Al-doped ZnO

3 Li Han,<sup>a\*</sup> Ngo Van Nong,<sup>a</sup> Le Thanh Hung,<sup>a</sup> Tim Holgate,<sup>a</sup> Nini Pryds,<sup>a</sup>  
4 Michitaka Ohtaki<sup>b</sup> and Søren Linderøth<sup>a</sup>

5 <sup>a</sup> Department of Energy Conversion and Storage, Technical University of  
6 Denmark, DTU Risø Campus, Frederiksborgvej 399, 4000 Roskilde, Denmark.

7 <sup>b</sup> Department of Molecular and Materials Sciences, Interdisciplinary Graduate  
8 School of Engineering Sciences, Kyushu University, 6-1 Kasugakoen, Kasuga,  
9 Fukuoka 816-8580, Japan

## 10 Abstract:

11 A systematic investigation on the microstructure and thermoelectric properties of Al-doped ZnO  
12 using  $\alpha$ - and  $\gamma$ -Al<sub>2</sub>O<sub>3</sub> as dopants was conducted in order to understand the doping effect and its  
13 mechanism. The samples were prepared by the spark plasma sintering technique from precursors  
14 calcined at various temperatures. Clear differences in microstructure and thermoelectric properties  
15 were observed between the samples doped with  $\alpha$ - and  $\gamma$ -Al<sub>2</sub>O<sub>3</sub>. At any given calcination  
16 temperature,  $\gamma$ -Al<sub>2</sub>O<sub>3</sub> resulted in the formation of a larger amount of the ZnAl<sub>2</sub>O<sub>4</sub> phase in the Al-  
17 doped ZnO samples. The average grain size was found to be smaller for the  $\gamma$ -Al<sub>2</sub>O<sub>3</sub>-doped  
18 samples than that for the  $\alpha$ -Al<sub>2</sub>O<sub>3</sub>-doped ones under the same sintering condition. It is proposed  
19 that the ZnAl<sub>2</sub>O<sub>4</sub> phase is the reason for the observed suppression of grain growth and also for the  
20 slightly reduced lattice thermal conductivity exhibited by these samples. The  $\gamma$ -Al<sub>2</sub>O<sub>3</sub> promoted the  
21 substitution for donor impurities in ZnO, thus resulting in shrinkage of the unit cell volume and an  
22 increase in the electrical conductivity compared with the  $\alpha$ -Al<sub>2</sub>O<sub>3</sub>-doped ZnO. At a calcination  
23 temperature of 1173K, the  $\gamma$ -Al<sub>2</sub>O<sub>3</sub>-doped sample showed a ZT value of 0.17 at 1173K, which is  
24 27% higher than that of the  $\alpha$ -Al<sub>2</sub>O<sub>3</sub>-doped sample.

25 *Key words: thermoelectric oxide, Al-doped ZnO,  $\alpha$ - and  $\gamma$ -Al<sub>2</sub>O<sub>3</sub>, ZnAl<sub>2</sub>O<sub>4</sub>*  
26 *formation kinetics.*

## 28 1. Introduction

29 Thermoelectric oxide materials are strong candidates for high temperature  
30 power generation from waste heat. The promising high temperature n-type

---

\* Corresponding author at: DTU Energy Conversion, DTU Risø Campus, Frederiksborgvej 399,  
4000 Roskilde, Denmark  
E-mail address: ihan@dtu.dk

thermoelectric properties of Al-doped ZnO were first brought to the public sight by Ohtaki et al. in 1996 [1]. Recently, a figure-of-merit, ZT of 0.44 at 1000 K was obtained for nanostructured Al-doped ZnO [2], and again this showed the possibility of using ZnO for low-cost practical waste heat harvesting. In the last few years, intensive investigations have been targeted to improve the thermoelectric properties and the preparation conditions of Al-doped ZnO [3,4,5,18], but little attention has been paid to the choice of which phases of  $\text{Al}_2\text{O}_3$  should be used as the dopant. This is probably one of the reasons for the controversial results reported by many research groups on the thermoelectric performance of Al-doped ZnO. Therefore, it is noteworthy to investigate systematically the influences of using different phases of  $\text{Al}_2\text{O}_3$  as dopants on the thermoelectric properties of Al-doped ZnO. In fact, the  $\alpha$ - and  $\gamma$ -phases of  $\text{Al}_2\text{O}_3$  have different crystal structures and physical properties with their specific reaction kinetics with ZnO [6,7,8]. Moreover, the phase transition of  $\text{Al}_2\text{O}_3$  is temperature dependent, suggesting that the synthesis temperature of Al-doped ZnO is crucial and can result in different material properties.

From this point of view, we have conducted a systematic investigation of the microstructure and the thermoelectric properties of Al-doped ZnO synthesized by various heat treatments using two different phases of  $\text{Al}_2\text{O}_3$  as dopants:  $\gamma$ - $\text{Al}_2\text{O}_3$  with a defect spinel structure and  $\alpha$ - $\text{Al}_2\text{O}_3$  with the corundum structure. We observed a noticeable difference in the microstructure and thermoelectric properties between  $\alpha$ - and  $\gamma$ - $\text{Al}_2\text{O}_3$ -doped ZnO when the synthesis temperature was lower than 1273 K. The correlations between the thermoelectric properties, microstructure evolutions, and the solid state reaction kinetics of the secondary phases are discussed herein.

## 2. Experimental Procedure

The starting materials used in these investigations are: ZnO (99+% 40-100 nm APS powder, Alfa-Aesar),  $\gamma$ - $\text{Al}_2\text{O}_3$  (99.5% 45-55 nm APS Powder, Alfa-Aesar), and  $\alpha$ - $\text{Al}_2\text{O}_3$  (99.5% 0.9-2.2 Micron APS Powder, Alfa-Aesar).

The synthesis of Al-doped ZnO ceramics: Aluminum oxide ( $\gamma$ - $\text{Al}_2\text{O}_3$  or  $\alpha$ - $\text{Al}_2\text{O}_3$ ) was mixed with ZnO at a molar ratio of 1:98 (the atomic ratio of Al:Zn = 2:98) by ethanol-aided roll milling using ceramic balls for 24 h. The resulting mixtures were then dried at room temperature for 24 h followed by further drying

at 403 K for 3 h. The dried powders were put into porcelain boats and calcined at various temperatures (973, 1073, 1173, and 1273 K) under  $N_2$  for 1 h. After calcination, the powders were sieved using a 300 mesh sieve, corresponding to a mean particle size of 48  $\mu m$ . The precursors were densified using optimized conditions into compact bulk pellets by spark plasma sintering (SPS) at 1173 K for 5 min in argon under a uniaxial pressure of 50 MPa. The six sintered samples are denoted as  $\gamma$ -973,  $\alpha$ -1073,  $\gamma$ -1073,  $\alpha$ -1173,  $\gamma$ -1173,  $\alpha$ -1273 according to the phase of  $Al_2O_3$  used and the calcination temperatures. These samples and their precursors were examined by power X-ray diffraction (XRD) on a Bruker D8 diffractometer (Bruker, Germany) using  $Cu-K\alpha$  radiation. The density of the samples was measured on an AccuPyc-1340 Pycnometer. A scanning electron microscope (SEM) (Supra, Carl Zeiss, Inc. Germany) equipped with an EDX spectrometer was used to observe the microstructures of the samples. The measurements of the electrical resistivity and the Seebeck coefficient were carried out on an ULVAC-RIKO ZEM-3 from room temperature up to 1173 K under a low pressure of helium atmosphere. The thermal conductivity was determined from the thermal diffusivity obtained by the laser flash method (a Netzch FLA-457) and the specific heat capacity calculated by the Dulong-Petit relation.

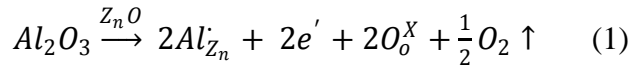
### 3. Results and discussion

The relative density of the bulk sintered ZnO samples doped with  $\alpha/\gamma$ - $Al_2O_3$  was found to be all above 95% regardless of the calcination temperature. X-ray diffraction analysis for these samples showed that most of the observed XRD peaks (see Fig. 1a) are assigned to those of pure ZnO phase (ICDD card PDF#36-1451). It also reveals in the inset of Fig. 1 that the peak at  $2\theta = 36.83^\circ$  assigned to the strongest peak of  $ZnAl_2O_4$  gahnite phase [14]. Comparing this peak over the samples, it seems as if those peaks of the  $\alpha$ -1073 and  $\gamma$ -973 samples are more diffused than those of the samples with higher calcination temperature. The cell volume monotonically decreased with increasing calcination temperature for both  $\alpha$ - and  $\gamma$ - $Al_2O_3$ -doped samples (see Fig. 1b). The ionic radius of  $Al^{3+}$  (0.039 nm, 4-fold coordination) is smaller than that of  $Zn^{2+}$  (0.060 nm, 4-fold coordination) [17], suggesting that the decrease of the unit cell volume may originate from the substitutions of  $Al^{3+}$  at Zn-sites promoted by the elevated calcination temperature.

96 It should also be noted that the unit cell volume was smaller for the  $\gamma$ -1073 and  $\gamma$ -  
97 1173 samples than that for the  $\alpha$ -1073 and  $\alpha$ -1173 samples, respectively.

98 Fig. 2a-f shows the SEM micrographs of fracture surfaces and the EDX  
99 analysis from a selected area of  $\alpha/\gamma$ -Al<sub>2</sub>O<sub>3</sub>-doped ZnO samples sintered by SPS.  
100 Fig. 2a-e reveal that besides the ZnO grains with the size of several micrometers,  
101 there exist some interspersed nano-sized grains, which precipitate within the ZnO  
102 grain interiors or at the grain boundaries. An EDX line scan was taken across the  
103 nanoprecipitates (see Figure 2e, f), showing that these nano-grains have enriched  
104 Al concentrations. This observation, together with the ZnAl<sub>2</sub>O<sub>4</sub> gahnite phase  
105 detected by XRD, suggests the formation of ZnAl<sub>2</sub>O<sub>4</sub> precipitates in these  
106 samples. A difference in the grain growth was also clearly observed as the  
107 calcination temperature increased. At the same calcination temperature the  $\gamma$ -  
108 Al<sub>2</sub>O<sub>3</sub>-doped samples have smaller average grain sizes ( $\sim 1\mu\text{m}$ ) than those of the  
109  $\alpha$ -Al<sub>2</sub>O<sub>3</sub>-doped samples ( $\sim 1.5\mu\text{m}$ ), as shown in Figs. 2b and 2c. This difference in  
110 grain size would be caused by the boundary pinning effect of the ZnAl<sub>2</sub>O<sub>4</sub>  
111 nanoprecipitates during grain growth [9]. These results indicate that the formation  
112 rate of ZnAl<sub>2</sub>O<sub>4</sub> is closely correlated to the phases of the Al<sub>2</sub>O<sub>3</sub> precursors, and  
113 this will be discussed in the following section with relation to the kinetic  
114 calculation.

115 Fig. 3 shows the temperature dependence of the electrical conductivity ( $\sigma$ ) of  
116  $\alpha/\gamma$ -Al<sub>2</sub>O<sub>3</sub>-doped ZnO samples. All the investigated samples showed a  
117 semiconducting behavior over the whole measured temperature range, i.e. the  
118 electrical conductivity increases with increasing temperature. The calculated  
119 activation energy for electronic conduction of the  $\alpha$ -1073 sample changed from  
120  $\sim 17$  meV to  $\sim 304$  meV at and above 770 K. With increasing calcination  
121 temperature, this change became less pronounced suggesting that more carriers  
122 are available for conduction. For both the  $\alpha$ - and the  $\gamma$ -Al<sub>2</sub>O<sub>3</sub>-doped ZnO samples,  
123 the electrical conductivity increased with increasing calcination temperature. The  
124  $\sigma$  values of the  $\gamma$ -1073 and  $\gamma$ -1173 samples are notably higher than those of the  $\alpha$ -  
125 1073 and  $\alpha$ -1173 samples, respectively. Shown in the inset of Fig. 3 is the  
126 electrical conductivity, which was extracted from the data at 1173 K, as a function  
127 of the calcination temperature. It appears that the change of  $\sigma$  is consistent with  
128 the change of the unit cell volume (Fig. 1b), which could be attributed to the Al  
129 substitution at the Zn-site according to the following equation [10]:



130

131 From Eq. 1, one can see that the substitution of  $Zn^{2+}$  by  $Al^{3+}$  is the reason for  
132 the unit cell volume shrinkage which may result in the increase in the donor  
133 impurity concentration [11], thus providing excess charged carriers available for  
134 electrical conduction.

135 Fig. 4 shows the temperature dependence of the Seebeck coefficients,  $S$ , of the  
136  $\alpha/\gamma$ - $Al_2O_3$ -doped samples. The  $S$  values of all the samples are negative over the  
137 whole temperature range examined, indicating n-type conduction. As shown in the  
138 inset of Fig. 4, at 1173 K, the  $\alpha/\gamma$ - $Al_2O_3$ -doped samples exhibit a monotonic  
139 decrease of  $S$  with increasing calcination temperature. According to Jonker and  
140 the Pisarenko relation, a simple broad band model for extrinsic n-type  
141 semiconductors with negligible hole conduction can describe this behavior [12],

$$\sigma = ne\mu \quad (2)$$

$$|S| = A'Tm_d^* \left(\frac{\pi}{3n}\right)^{2/3} \quad (3)$$

142

143 where  $n$  is the carrier concentration,  $e$  is the electric charge of the carrier,  $\mu$  is the  
144 mobility,  $A'$  is a constant,  $T$  is the absolute temperature,  $m_d^*$  is a density of the  
145 state (DOS) effective mass at the Fermi level. As the electrical conductivity ( $\sigma$ )  
146 and the Seebeck coefficient ( $S$ ) are both a function of the carrier concentration ( $n$ ),  
147 Eq. 2 and 3 clearly show that a higher  $n$  value causes an increase in  $\sigma$  but a  
148 decrease in  $|S|$ , which well explains the tendency observed in Fig.4. For example,  
149 the  $\alpha$ -1273 sample with the highest electrical conductivity showed the smallest  $|S|$   
150 in the investigated temperature region.

151 The total thermal conductivity ( $\kappa$ ) of the sintered samples using different  $\alpha/\gamma$ -  
152  $Al_2O_3$  and various calcination temperatures is shown in Fig. 5. In general,  $\kappa$   
153 rapidly decreases with increasing temperature, which is in good agreement with  
154 the result reported by Ohtaki et al [13]. It can also be seen from Fig. 5 that  $\kappa$  tends  
155 to increase with increasing calcination temperature. We estimated the electronic  
156 contribution  $\kappa_e$  using the Wiedemann–Franz law and found that the increase in  $\kappa$   
157 with increasing calcination temperature is attributed to the increase in  $\kappa_e$ ,  
158 particularly in the high temperature region. Although the total  $\kappa$  values at 1173 K



as a function of the calcination temperature (see Fig. 5 inset) appeared to be virtually the same for both  $\alpha$ - and  $\gamma$ - $\text{Al}_2\text{O}_3$ -doped samples, the lattice thermal conductivity,  $\kappa_L$ , of the samples at 1173 K was somewhat smaller for the  $\gamma$ -1073 and  $\gamma$ -1173 samples ( $5.06 \text{ Wm}^{-1}\text{K}^{-1}$  and  $5.15 \text{ Wm}^{-1}\text{K}^{-1}$ , respectively) than those of the  $\alpha$ -1073  $\alpha$ -1173 samples ( $5.31 \text{ Wm}^{-1}\text{K}^{-1}$  and  $5.43 \text{ Wm}^{-1}\text{K}^{-1}$ , respectively). As illustrated by the microstructure in Fig. 2, the reason for the lower conductivity in the  $\gamma$ -1073 sample as compared with the  $\alpha$ -1073 sample is probably due to the formation of disperse  $\text{ZnAl}_2\text{O}_4$  nanoprecipitates in  $\gamma$ -1073 sample which might act as a phonon scattering center.

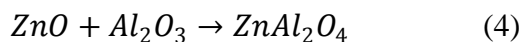
The power factor,  $S^2\sigma$ , of the samples is presented in Fig. 6. It shows that the power factor values of  $\gamma$ -1073 and  $\gamma$ -1173 are notably higher than that of  $\alpha$ -1073 and  $\alpha$ -1173. Also, the power factor monotonically increases with increasing calcination temperature, as shown in the inset of Fig. 6. The higher power factor observed for the  $\gamma$ - $\text{Al}_2\text{O}_3$ -doped samples was mainly due to the increase in their electrical conductivity as compared to that of the  $\alpha$ - $\text{Al}_2\text{O}_3$ -doped samples. At 1173K, the highest power factor of  $\sim 8.31 \times 10^{-4} \text{ Wm}^{-1}\text{K}^{-2}$  measured in this study is comparable to the value of  $\sim 8 - 15 \times 10^{-4} \text{ Wm}^{-1}\text{K}^{-2}$  reported by Ohtaki et al [1] and the value of  $\sim 8.3 \times 10^{-4} \text{ Wm}^{-1}\text{K}^{-2}$  reported by Jood et al [2] for Al-doped ZnO.

The dimensionless figure of merit,  $ZT$ , is given in Fig. 7, showing that the  $ZT$  values of  $\gamma$ -1073 and  $\gamma$ -1173 are also higher than those of  $\alpha$ -1073 and  $\alpha$ -1173. At 1173K, the  $\gamma$ -1173 sample with the highest power factor attained a  $ZT$  of 0.17, which is about 27% higher than that for the  $\alpha$ - $\text{Al}_2\text{O}_3$ -doped counterpart at the same temperature. The highest  $ZT$  value of our sample is on the same order of the one reported by Ohtaki et al [1] at the same temperature. It should be noted here that the higher  $ZT$  value ( $ZT \sim 0.44$  at 1000 K) reported by Jood et al is mainly due to the suppression in the thermal conductivity of the sample by nanostructuring [2]. Nevertheless, our  $ZT$  value is higher than the ones reported by Cai et al [10] and Tanaka et al [16] at the same temperature.

We found that the ZnO samples doped with  $\gamma$ - $\text{Al}_2\text{O}_3$  showed a better thermoelectric performance compared to those doped with  $\alpha$ - $\text{Al}_2\text{O}_3$ , when calcined at a temperature lower than 1273 K. At a calcination temperature higher than 1273 K, the difference in the thermoelectric properties gradually diminishes due to the intrinsic phase transformation of  $\gamma$ - $\text{Al}_2\text{O}_3$  to  $\alpha$ - $\text{Al}_2\text{O}_3$ .



192 To understand these observations, we looked into the kinetics and mechanism  
193 of the reaction between ZnO and Al<sub>2</sub>O<sub>3</sub>. The formation of the secondary phase,  
194 ZnAl<sub>2</sub>O<sub>4</sub>, resulting from the reaction between ZnO and Al<sub>2</sub>O<sub>3</sub> is well known, and  
195 can be represented as follows:



196 It should be noted that the formation of ZnAl<sub>2</sub>O<sub>4</sub> cannot be avoided during the  
197 preparation process of Al-doped ZnO [2,4,5]. The limited solubility of Al atom  
198 into ZnO [14] could be one of the reasons. According to the thermodynamics  
199 description of the reaction (Eq. 4) suggested by K. T. Jacob [6], the standard  
200 Gibbs free energy change ( $\Delta G$ ) of the ZnAl<sub>2</sub>O<sub>4</sub> formation from the reaction of  $\alpha$ -  
201 Al<sub>2</sub>O<sub>3</sub> and ZnO equals  $-45.0081 + 0.0066T$  kJ, indicating that the formation of  
202 ZnAl<sub>2</sub>O<sub>4</sub> is favored from room temperature to far above 1673 K ( $\Delta G \leq 0$ ). The  
203 reaction rate is kinetically controlled by solid state diffusion [7,8].

205 Fig. 8 shows the calculated reaction time course of ZnAl<sub>2</sub>O<sub>4</sub> formation using  
206 Jander's model for powder reactions. According to this model, it is assumed that  
207 Al<sub>2</sub>O<sub>3</sub> particles are embedded in a quasi-continuous ZnO medium. The reaction  
208 rate of the ZnAl<sub>2</sub>O<sub>4</sub> formation from ZnO and Al<sub>2</sub>O<sub>3</sub> is diffusion-controlled and  
209 hence follows a parabolic rate law:

$$\left[1 - (1 - W)^{\frac{1}{3}}\right]^2 = 2 \cdot k_p \cdot t / r_o^2 \quad (5)$$

210 where  $W$  is the weight fraction of the reacted Al<sub>2</sub>O<sub>3</sub>,  $k_p$  is the practical parabolic  
211 rate constant,  $t$  is the reaction time and  $r_o$  is the particle size of Al<sub>2</sub>O<sub>3</sub> powder. The  
212 practical parabolic rate constant  $k_p$  follows the Arrhenius law:  
213

$$k_p = A \cdot e^{-\frac{E_a}{RT}} \quad (6)$$

214 where  $A$  is pre-exponential factor (a term which includes factors like the  
215 frequency of collisions and their orientation),  $E_a$  is the activation energy,  $R$  is the  
216 gas constant,  $T$  is temperature. By combining Eq. 5 and Eq. 6, one can obtain:  
217

$$W = 1 - \left[1 - (2A \cdot t)^{\frac{1}{2}} \cdot e^{-\frac{E_a}{2RT}} \cdot r_o^{-1}\right]^3 \quad (7)$$

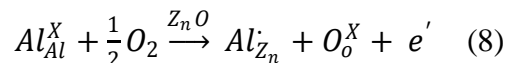
218 According to the experimental data reported by Tsuchida et al [8], the parameters  
219 of  $A$  and  $E_a$  can be obtained by Arrhenius fitting.  $A$  equals  $18076 \mu\text{m}^2 \text{min}^{-1}$ .  $E_a$  for  
220  $\alpha$ -Al<sub>2</sub>O<sub>3</sub> and  $\gamma$ -Al<sub>2</sub>O<sub>3</sub> equals 4.9 and 2.04 eV, respectively.  $r_o$  equals the average  
221 particle size of Al<sub>2</sub>O<sub>3</sub> powder. Using Eq. 7, the reacted Al<sub>2</sub>O<sub>3</sub> fraction can be  
222

223 plotted as a function of time. As shown in Fig. 8a, the reaction rate of  $\gamma$ - $\text{Al}_2\text{O}_3$   
 224 with ZnO is significantly higher than that of  $\alpha$ - $\text{Al}_2\text{O}_3$  at the same temperature due  
 225 to the lower activation energy of  $\gamma$ - $\text{Al}_2\text{O}_3$ . From these data, we calculated the  
 226 percentage of reaction completed after 1 hour as a function of the calcination  
 227 temperature, and the results are shown in Fig. 8b. A clear correlation was found  
 228 between the percentage of the reacted  $\text{Al}_2\text{O}_3$  and the thermoelectric properties of  
 229 these samples. The  $\alpha$ -1073 sample with the smallest calculated percentage of the  
 230 reacted  $\text{Al}_2\text{O}_3$  showed the lowest  $\sigma$  values, while the  $\alpha$ -1273 and  $\gamma$ -1173 samples  
 231 with almost fully reacted  $\text{Al}_2\text{O}_3$  showed relatively high  $\sigma$ . Accordingly, the  
 232 electrical conductivities of the  $\gamma$ -1073/1173 samples were higher than those of the  
 233  $\alpha$ -1073/1173 samples (Fig. 3). Also, the smaller grains size of the  $\gamma$ - $\text{Al}_2\text{O}_3$ -doped  
 234 samples compared to that of the  $\alpha$ - $\text{Al}_2\text{O}_3$ -doped ones may be explained by a  
 235 stronger boundary pinning effect during grain growth caused by a larger number  
 236 of  $\text{ZnAl}_2\text{O}_4$  nanoprecipitates. This is presumably due to the faster reaction and  
 237 larger fraction of  $\text{ZnAl}_2\text{O}_4$  formation for the  $\gamma$ - $\text{Al}_2\text{O}_3$ -doped samples.

238 The detailed mechanisms of the reaction between ZnO and  $\text{Al}_2\text{O}_3$  have already  
 239 been studied by Branson [7] and Tsuchida et al [8]. Branson carried out marker  
 240 transport experiments at the interfaces between ZnO,  $\text{ZnAl}_2\text{O}_4$  and  $\text{Al}_2\text{O}_3$ , and  
 241 pointed out that the formation of  $\text{ZnAl}_2\text{O}_4$  is a result of Zn ions diffusing into  
 242  $\text{Al}_2\text{O}_3$ . Later, Tsuchida et al. not only showed evidence to support this result but  
 243 also revealed the reason for the  $\text{ZnAl}_2\text{O}_4$  formation speed. They pointed out that  
 244 the reaction of  $\alpha$  or  $\gamma$ - $\text{Al}_2\text{O}_3$  with ZnO resulted in different degrees of crystallinity  
 245 of the product layers, i.e. formation of  $\text{ZnAl}_2\text{O}_4$  as “hereditary structure” [8].  
 246 Owing to the different degrees of crystallinity, the diffusivity of Zn ions in  
 247  $\text{ZnAl}_2\text{O}_4$  can be varied. As a result, in the  $\gamma$ - $\text{Al}_2\text{O}_3$ , the formation of a defect  
 248  $\text{ZnAl}_2\text{O}_4$  layer with a higher diffusivity of the Zn ions is observed.  
 249 Correspondingly,  $\alpha$ - $\text{Al}_2\text{O}_3$  results in a nearly perfect, defect free  $\text{ZnAl}_2\text{O}_4$  structure  
 250 with a lower diffusivity of the Zn ions and higher activation energy.

251 However, the faster formation of the  $\text{ZnAl}_2\text{O}_4$  phase is not likely to be the  
 252 direct reason for the increase of the electrical conductivity in the  $\gamma$ - $\text{Al}_2\text{O}_3$ -doped  
 253 samples, since the  $\text{ZnAl}_2\text{O}_4$  phase is reported to be unfavorable for the electrical  
 254 conductivity [1]. By comparing Fig. 1b and 8b, the unit cell volume shrinkage  
 255 increases along with increasing the  $\text{ZnAl}_2\text{O}_4$  phase formation, indicating that the

substitution of Al for Zn simultaneously occurred during the formation of the ZnAl<sub>2</sub>O<sub>4</sub> phase, which can be represented as:



According to the previous investigations by Branson, the diffusion of Al toward ZnO does not contribute to the formation of ZnAl<sub>2</sub>O<sub>4</sub> [7]. His explanation of the reaction between ZnO and Al<sub>2</sub>O<sub>3</sub> did not take the Al diffusion into consideration. From our experimental results and investigations by other groups who observed the existence of Al diffusion into ZnO using HRTEM [15], a modified Branson's schematic diagram of the reaction process is proposed and the details is presented in Fig. 9. It includes a counter-diffusion between ZnO and Al<sub>2</sub>O<sub>3</sub>. The formation of ZnAl<sub>2</sub>O<sub>4</sub> is only caused by the diffusion of Zn to Al<sub>2</sub>O<sub>3</sub>, while the Al substitution for Zn results from the diffusion of Al into ZnO. The disordered structure of  $\gamma$ -Al<sub>2</sub>O<sub>3</sub> may lead to the disordered product layers of ZnAl<sub>2</sub>O<sub>4</sub>. The Al and Zn ions would be easier to diffuse through the disordered product layer. It promotes both the formation of ZnAl<sub>2</sub>O<sub>4</sub> and the substitutions of Al for Zn as donor impurities in ZnO, thus resulting in enhanced grain boundary pinning by ZnAl<sub>2</sub>O<sub>4</sub> and the observed higher electrical conductivity of the  $\gamma$ -Al<sub>2</sub>O<sub>3</sub>-doped ZnO than that of the  $\alpha$ -Al<sub>2</sub>O<sub>3</sub>-doped counterpart.

## 4. Conclusions

In summary, we observed a close correlation between the thermoelectric properties, microstructure evolution, and the solid state reaction kinetics of the ZnAl<sub>2</sub>O<sub>4</sub> formation using Jander's solid-state reaction model. At a given calcinations temperature, the addition of  $\gamma$ -Al<sub>2</sub>O<sub>3</sub> resulted in a larger fraction of the ZnAl<sub>2</sub>O<sub>4</sub> formation in the Al-doped ZnO samples, which also inhibited the grain growth and slightly reduced the lattice thermal conductivity. The higher diffusion rate of Al observed for the  $\gamma$ -Al<sub>2</sub>O<sub>3</sub> resulted in a larger unit cell volume shrinkage and higher electrical conductivity as compared with the  $\alpha$ -Al<sub>2</sub>O<sub>3</sub>-doped ZnO. As a consequence,  $\gamma$ -Al<sub>2</sub>O<sub>3</sub>-doped ZnO exhibited a higher ZT than the  $\alpha$ -Al<sub>2</sub>O<sub>3</sub>-doped counterpart under the same preparation conditions with calcination temperatures lower than 1273 K.

## 286 Acknowledgements

287 The authors would like to thank the Programme Commission on Energy and Environment (EnMi)  
288 which is part of the Danish Council for Strategic Research (Contract No. 10-093971) for  
289 sponsoring the OTE-POWER research work.

## 290 References

- 291 [1] M. Ohtaki, T. Tsubota, K. Eguchi, H. Arai, High-temperature thermoelectric properties of  $(\text{Zn}_{1-x}\text{Al}_x)\text{O}$ , *J. Appl. Phys.* 79 (1997) 1816-1818.
- 292
- 293 [2] P. Jood, R. J. Mehta, Y. Zhang, G. Peleckis, X. Wang, R. W. Siegel, T. Borca-Tasciuc, S. X.  
294 Dou, G. Ramanath, Al-doped zinc oxide nanocomposites with enhanced thermoelectric properties,  
295 *Nano Lett.* 11 (2011) 4337-4342.
- 296 [3] K. H. Kim, S. H. Shim, K. B. Shim, Microstructural and thermoelectric characteristics of zinc  
297 oxide-based thermoelectric materials fabricated using a spark plasma sintering process, *J. Am.*  
298 *Ceram. Soc.* 88 (2005) 628-632.
- 299 [4] N. Ma, J. F. Li, B. P. Zhang, Y. H. Lin, L. R. Ren, G. F. Chen, Microstructure and  
300 thermoelectric properties of  $\text{Zn}_{1-x}\text{Al}_x\text{O}$  ceramics fabricated by spark plasma sintering, *J. Phys. and*  
301 *Chem. of Solids* 71 (2012) 1344-1349.
- 302 [5] D. Berardan, C. Byl, N. Dragoë, Influence of the preparation conditions on the thermoelectric  
303 properties of Al-doped ZnO, *J. Am. Ceram. Soc.* 93 (2010) 2352-2358.
- 304 [6] K. T. Jacob, Gibbs free energies of formation of  $\text{ZnAl}_2\text{O}_4$  and  $\text{ZnCr}_2\text{O}_4$ , *Thermochimica Acta*  
305 15 (1976) 79-87.
- 306 [7] D. L. Branson, Kinetics and mechanism of the reaction between zinc oxide and aluminum  
307 oxide, *J. Am. Ceram. Soc.* 48 (1965) 591.
- 308 [8] T. Tsuchida, R. Furuichi, T. Ishii, Reactivity of  $\eta$ -,  $\gamma$ -, and  $\alpha$ - $\text{Al}_2\text{O}_3$  for  $\text{ZnAl}_2\text{O}_4$  formation, *Z*  
309 *anorg. Allg. Chem.* 415 (1975) 175-184.
- 310 [9] N. Moelans, B. Blanpain, P. Wollants, Pinning effect of second-phase particles on grain growth  
311 in polycrystalline films studied by 3-D phase field simulations, *Acta Mater.* 55 (2007) 2173-2182.
- 312 [10] K. F. Cai, E. Muller, C. Drasar, A. Mrozek Preparation and thermoelectric properties of Al-  
313 doped ZnO ceramics, *Mater. Sci. Eng. B* 104 (2003) 45-48.
- 314 [11] A. E. Jimenez-Gonzalez, J. A. S. Urueta, R. Suarez-Parra, Optical and electrical  
315 characteristics of aluminum-doped ZnO thin films prepared by solgel technique, *J. Cryst. Growth*  
316 192 (1998) 430-438.
- 317 [12] M. Y. Su, C. E. Elsbernd, T. O. Mason, Jonker 'Pear' Analysis of Oxide Superconductors, *J.*  
318 *Am. Ceram. Soc.* 73 (1990) 415-419.
- 319 [13] M. Ohtaki, K. Araki, K. Yamamoto, High thermoelectric performance of dually doped ZnO  
320 ceramics, *J. Electron Mater.* 38 (2009) 1234.
- 321 [14] H. Serier, M. Gaudon, M. Ménétrier, Al-doped ZnO powdered materials: Al solubility limit  
322 and IR absorption properties, *Solid State Sci.* 11 (2009) 1192-1197.

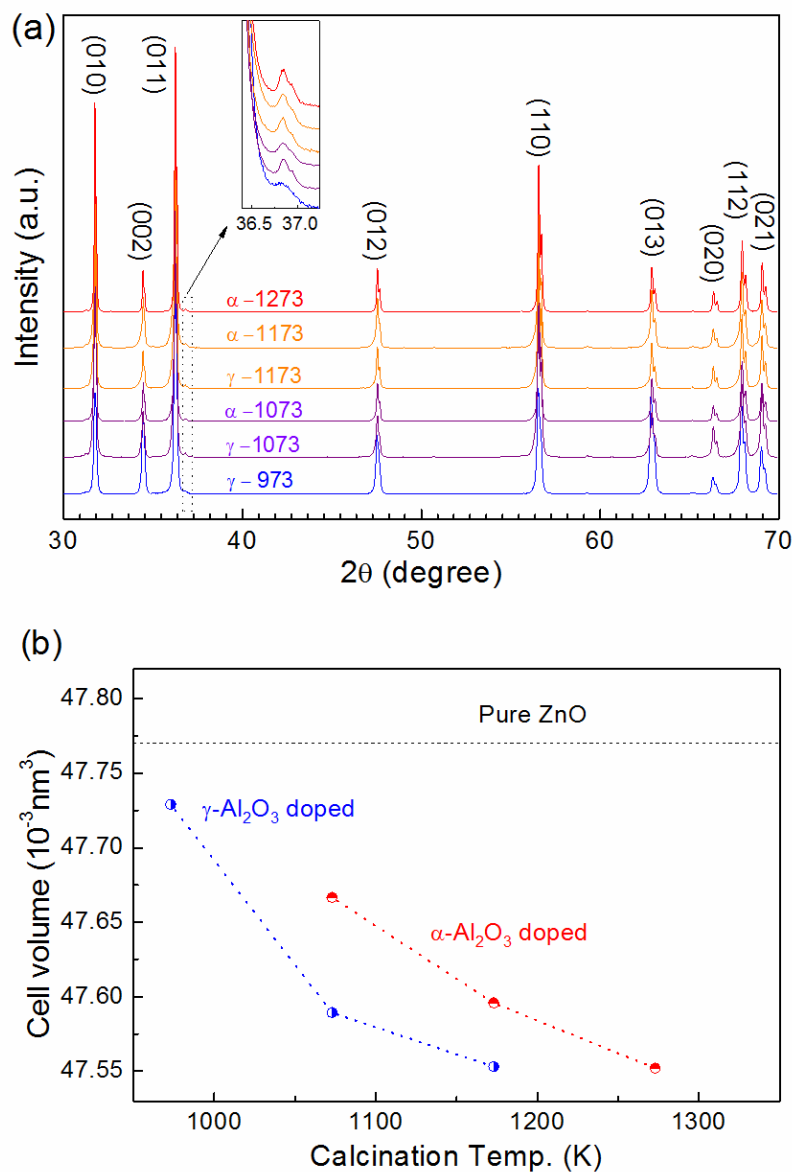
- [15] Y. Kinemuchi, H. Nakano, H. Kaga, S. Tanaka, K. Uematsu, K. Watari, Microstructural evidence of hall mobility anisotropy in c-axis textured Al-doped ZnO, *J. Am. Ceram. Soc.* 94 (2011) 2339-2343.
- [16] Y. Tanaka, T. Ifuku, K. Tsuchida, A. Kato, Thermoelectric properties of ZnO-based materials, *J. Mater. Sci. Lett.* 16 (1997) 155.
- [17] R. D. Shannon, Revised Effective Ionic Radii and Systematic studies of interatomic distances in halides and chalcogenides, *Acta Cryst. A* 32 (1976) 751.
- [18] N. Vogel-Schäuble, Y. E. Romanyuk, S. Yoon, K. J. Saji, S. Populoh, S. Pokrant, M. H. Aguirre, A. Weidenkaff, Thermoelectric properties of nanostructured Al-substituted ZnO thin films, *thin solid film* 520 (2012) 6869-6875.

## Figure captions

- Fig. 1. (a) XRD patterns of  $\alpha/\gamma$ -Al<sub>2</sub>O<sub>3</sub>-doped ZnO with different calcination temperatures (from 973 to 1273 K). The dotted box magnified as the inset shows the position of the strongest peak from ZnAl<sub>2</sub>O<sub>4</sub>. (b) The unit cell volume obtained from the lattice parameter refinement as a function of the calcination temperature.
- Fig. 2. SEM photographs of the fracture surfaces of  $\alpha/\gamma$ -Al<sub>2</sub>O<sub>3</sub>-doped ZnO. (a)  $\gamma$ -973, (b)  $\gamma$ -1073, (c)  $\alpha$ -1073, (d)  $\alpha$ -1273, (e) a representative high-magnification SEM image of the ZnAl<sub>2</sub>O<sub>4</sub> nanoprecipitates. EDX line scans of Zn, O, and Al K $\alpha_1$  X-ray peaks obtained along the yellow arrow are shown in (f).
- Fig. 3. Temperature dependence of the electrical conductivity of  $\alpha/\gamma$ -Al<sub>2</sub>O<sub>3</sub>-doped ZnO samples. The inset shows the electrical conductivity at 1173 K as a function of the calcination temperature.
- Fig. 4. Temperature dependence of the Seebeck coefficient of  $\alpha/\gamma$ -Al<sub>2</sub>O<sub>3</sub>-doped ZnO samples. The inset shows the Seebeck coefficient at 1173 K as a function of the calcination temperature.
- Fig. 5. Temperature dependence of the thermal conductivity of  $\alpha/\gamma$ -Al<sub>2</sub>O<sub>3</sub>-doped ZnO samples. The inset shows the thermal conductivity at 1173 K as a function of the calcination temperature.
- Fig. 6. Temperature dependence of the power factor of  $\alpha/\gamma$ -Al<sub>2</sub>O<sub>3</sub>-doped ZnO samples. The inset shows the power factor at 1173 K as a function of the calcination temperature.
- Fig. 7. Temperature dependence of ZT of  $\alpha/\gamma$ -Al<sub>2</sub>O<sub>3</sub>-doped ZnO samples. The inset shows the ZT values at 1173 K as a function of the calcination temperature.
- Fig.8. (a) The calculated reaction time course as a weight fraction of reacted Al<sub>2</sub>O<sub>3</sub> for the ZnAl<sub>2</sub>O<sub>4</sub> formation. (b) The percentage of reaction completed after 1 hour as a function of the calcination temperature.
- Fig. 9. A modified schematic diagram for the solid-state reaction process of ZnO and Al<sub>2</sub>O<sub>3</sub> based on Branson's investigation.

359

360 Fig. 1

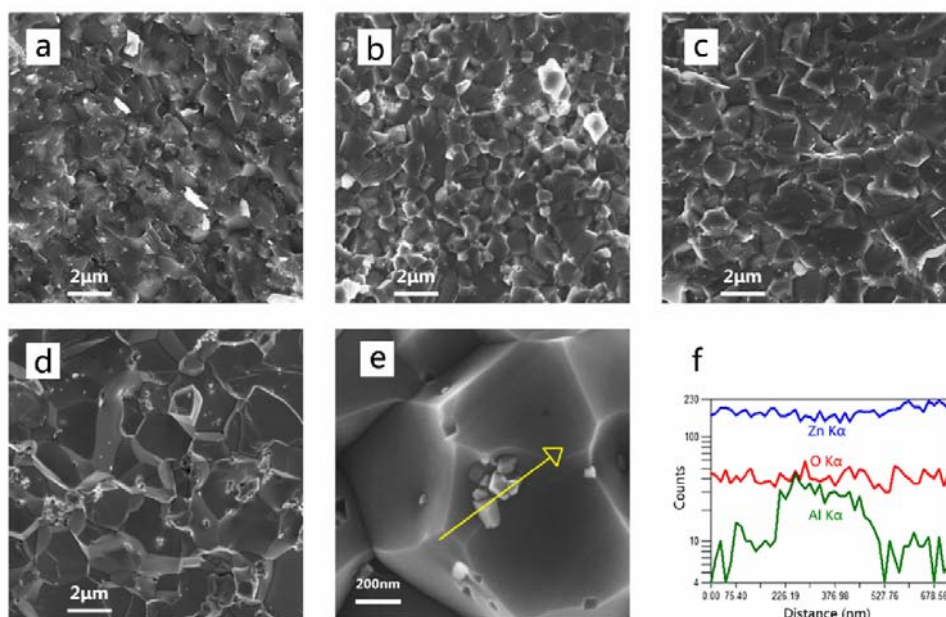


361

362 Fig. 1. (a) XRD patterns of  $\alpha/\gamma$ - $\text{Al}_2\text{O}_3$ -doped ZnO with different calcination temperatures (from  
363 973 to 1273 K). The dotted box magnified as the inset shows the position of the strongest peak  
364 from  $\text{ZnAl}_2\text{O}_4$ . (b) The unit cell volume obtained from the lattice parameter refinement as a  
365 function of the calcination temperature.

366

367 Fig. 2



368

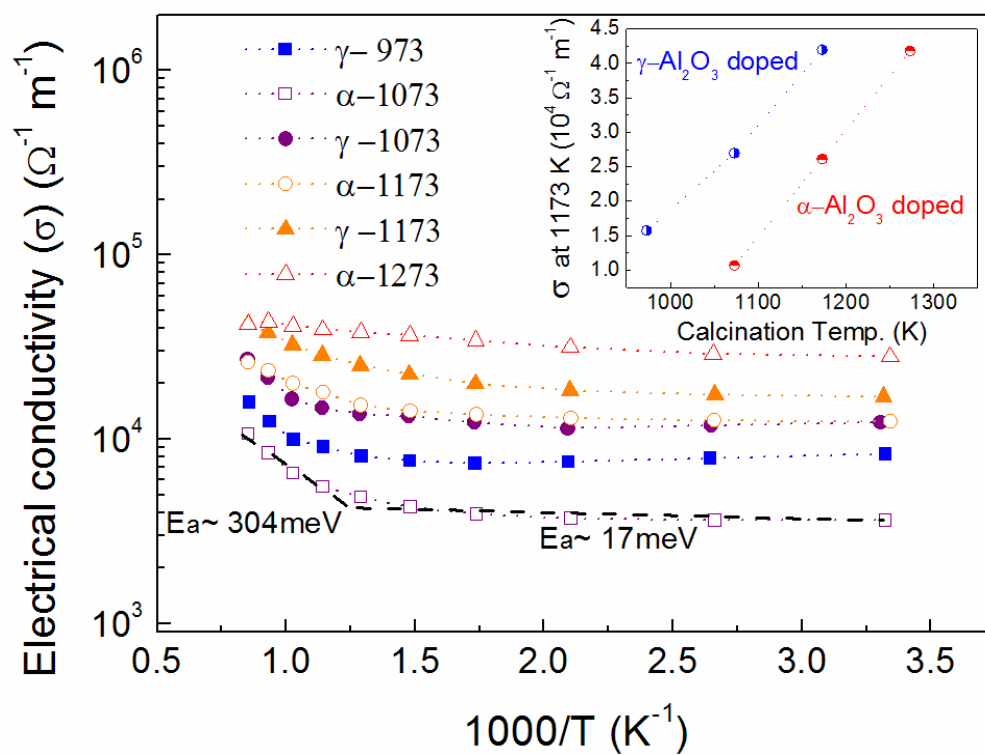
369 Fig. 2. SEM photographs of the fracture surfaces of  $\alpha/\gamma$ - $\text{Al}_2\text{O}_3$ -doped ZnO. (a)  $\gamma$ -973, (b)  $\gamma$ -1073,370 (c)  $\alpha$ -1073, (d)  $\alpha$ -1273, (e) a representative high-magnification SEM image of the  $\text{ZnAl}_2\text{O}_4$ 371 nanoprecipitates. EDX line scans of Zn, O, and Al  $\text{K}\alpha_1$  X-ray peaks obtained along the yellow

372 arrow are shown in (f).

373



374 Fig. 3



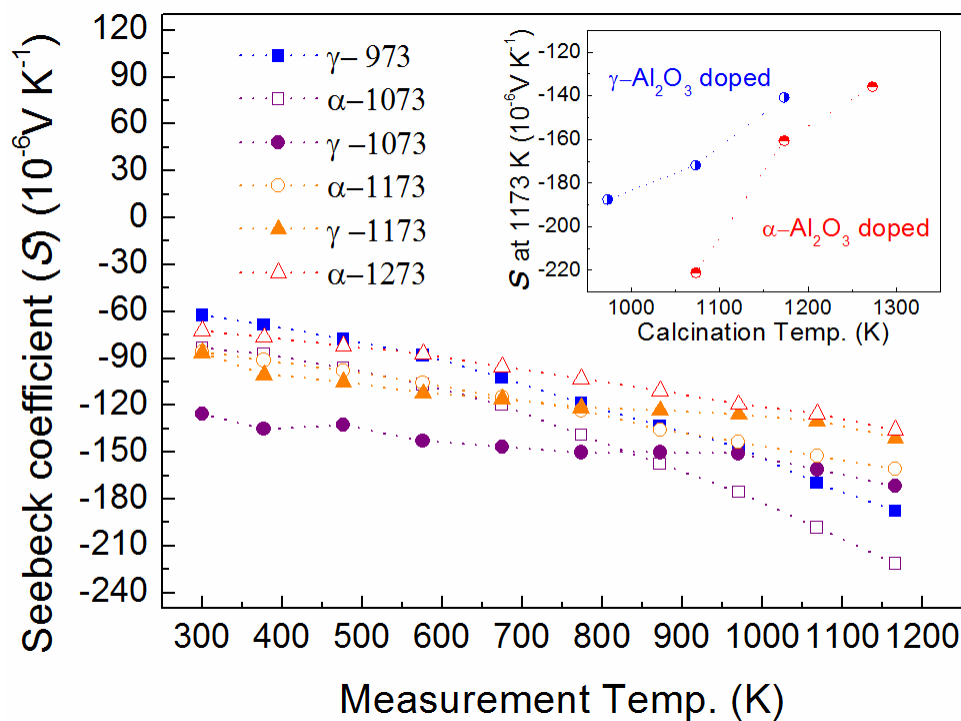
375

376 Fig. 3. Temperature dependence of the electrical conductivity of  $\alpha/\gamma$ - $\text{Al}_2\text{O}_3$ -doped ZnO samples.

377 The inset shows the electrical conductivity at 1173 K as a function of the calcination temperature.

378

379 Fig. 4



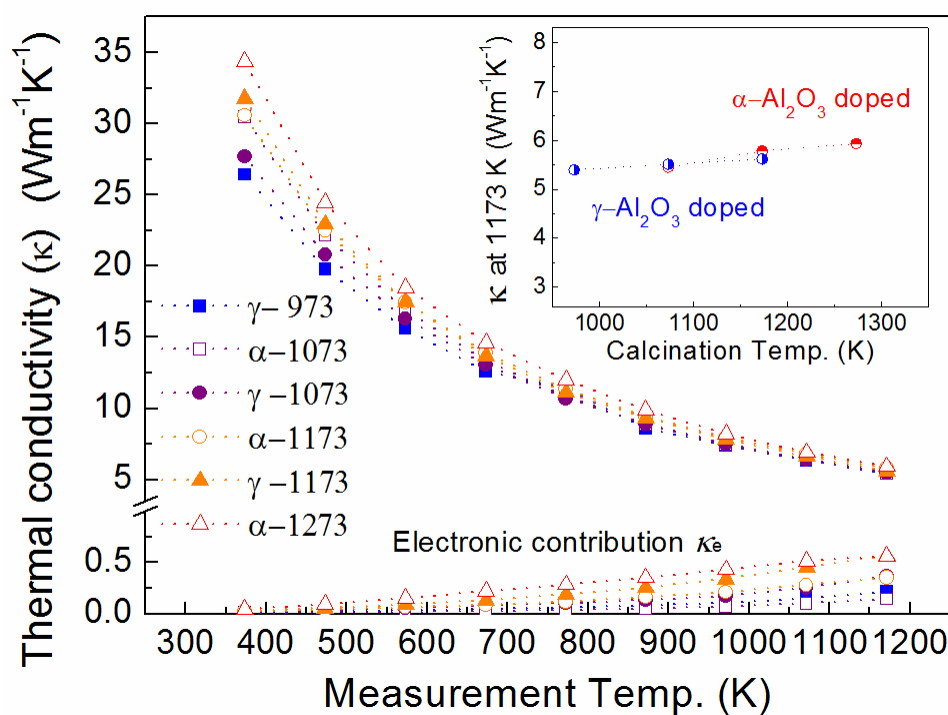
380

381 Fig. 4. Temperature dependence of the Seebeck coefficient of  $\alpha/\gamma$ - $\text{Al}_2\text{O}_3$ -doped ZnO samples. The  
 382 inset shows the Seebeck coefficient at 1173 K as a function of the calcination temperature.

383

384 Fig. 5

385



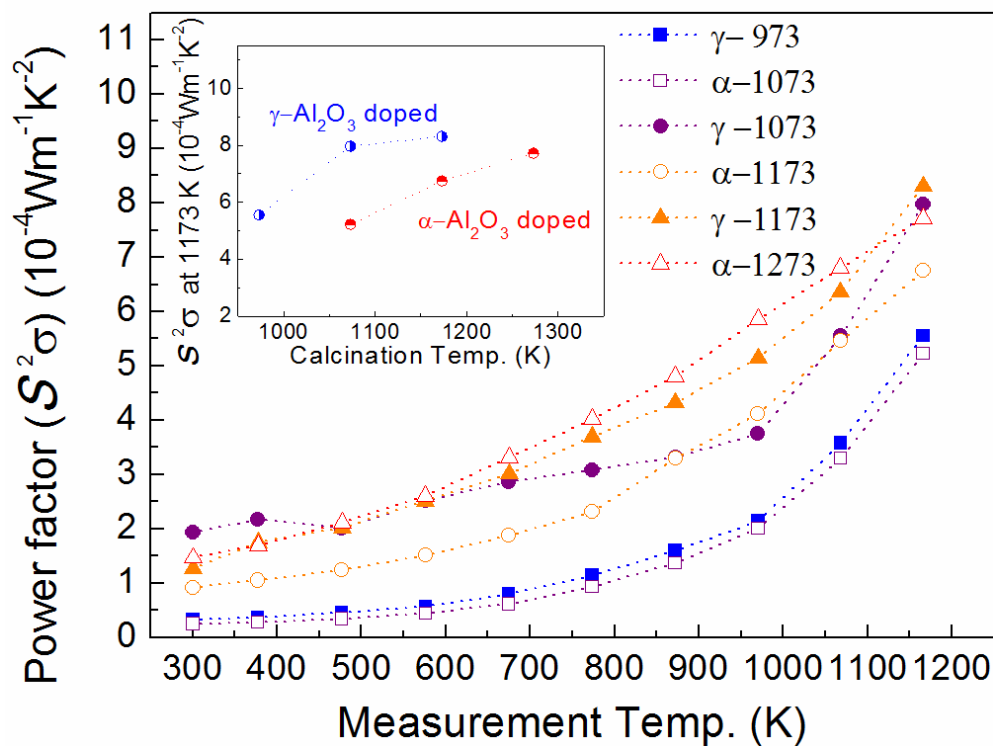
386

387 Fig. 5. Temperature dependence of the thermal conductivity of  $\alpha/\gamma\text{-Al}_2\text{O}_3$ -doped ZnO samples.

388 The inset shows the thermal conductivity at 1173 K as a function of the calcination temperature.

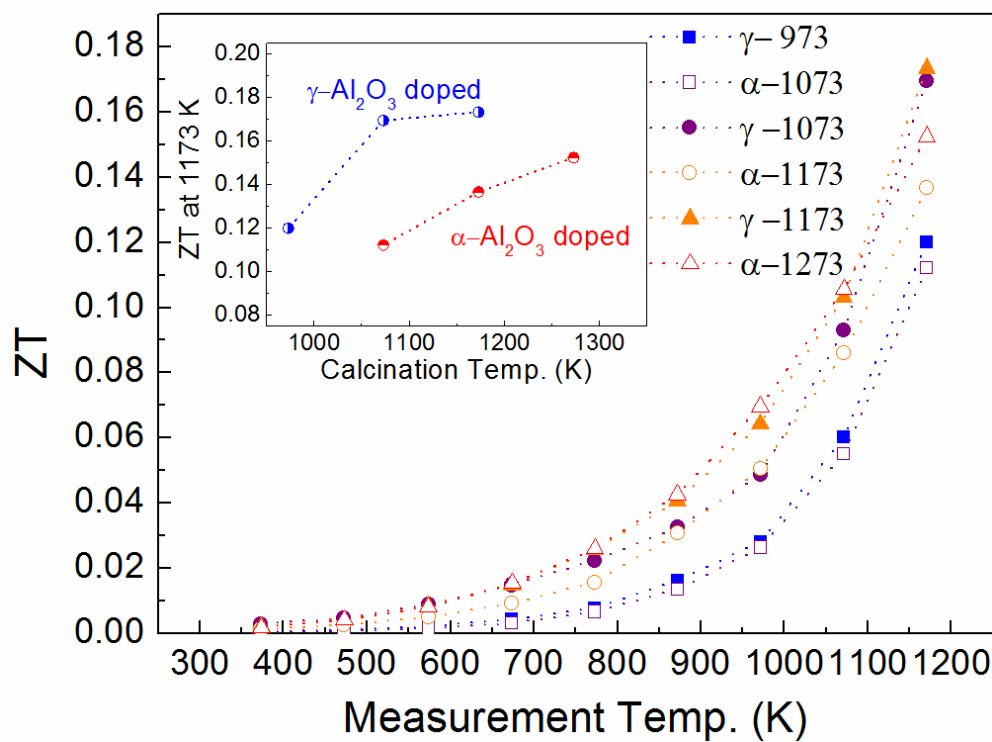
389

390 Fig. 6



391  
392 Fig. 6. Temperature dependence of the power factor of  $\alpha/\gamma$ - $\text{Al}_2\text{O}_3$ -doped ZnO samples. The inset  
393 shows the power factor at 1173 K as a function of the calcination temperature.  
394

395 Fig. 7



396

397 Fig. 7. Temperature dependence of ZT of  $\alpha/\gamma$ - $\text{Al}_2\text{O}_3$ -doped ZnO samples. The inset shows the ZT  
 398 values at 1173 K as a function of the calcination temperature.

399

400 Fig. 8

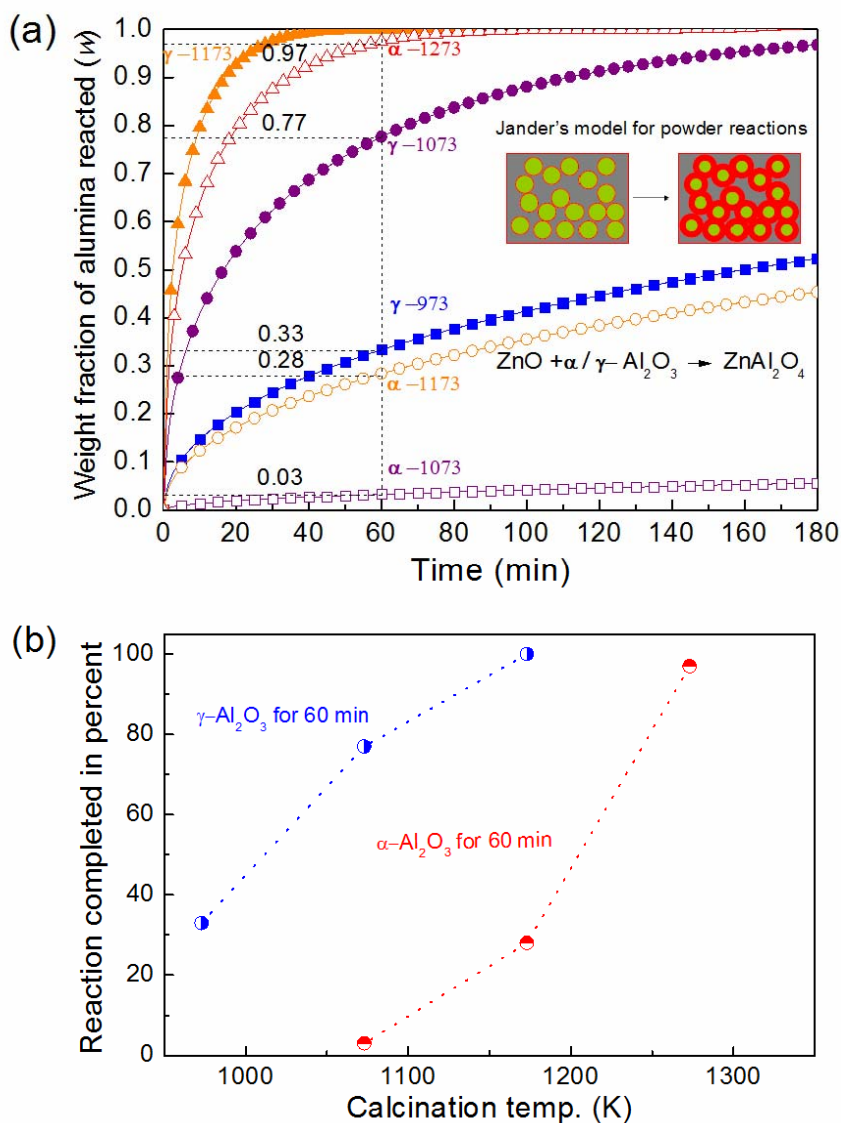
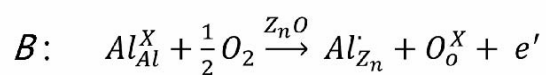
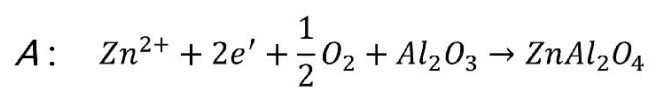
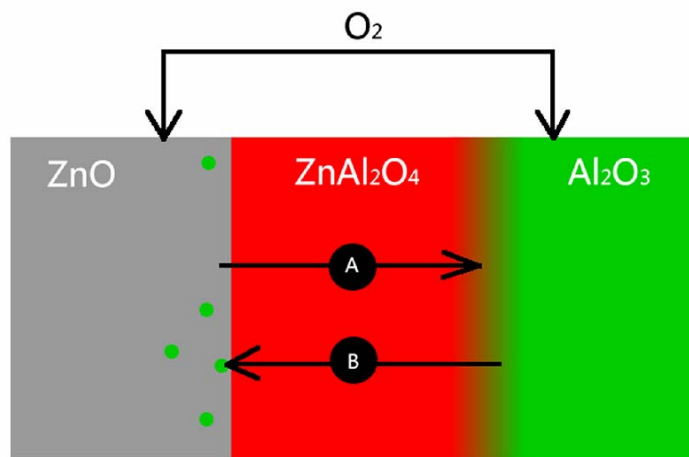


Fig.8. (a) The calculated reaction time course as a weight fraction of reacted  $\text{Al}_2\text{O}_3$  for the  $\text{ZnAl}_2\text{O}_4$  formation. (b) The percentage of reaction completed after 1 hour as a function of the calcination temperature.

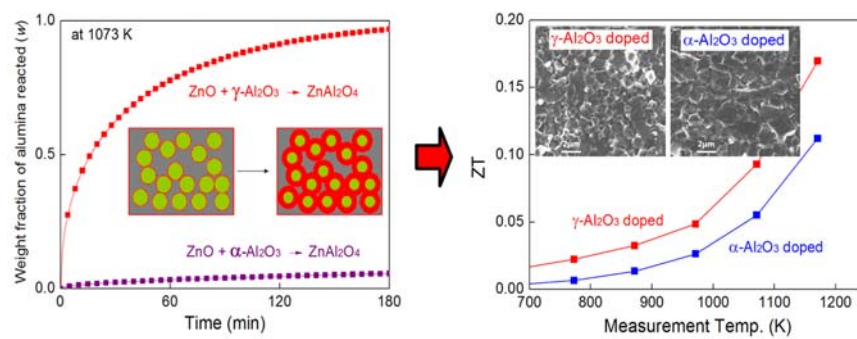
407 Fig. 9



408

409 Fig. 9. A modified schematic diagram for the solid-state reaction process of ZnO and Al<sub>2</sub>O<sub>3</sub> based  
 410 on Branson's investigation.





411

## Highlights

412

413

414

415

416

417

418

419

420

421

422

- Clear differences in microstructure and thermoelectric properties were observed between the  $\gamma$ -Al<sub>2</sub>O<sub>3</sub>-doped ZnO and  $\alpha$ -Al<sub>2</sub>O<sub>3</sub>-doped ZnO.
- $\gamma$ -Al<sub>2</sub>O<sub>3</sub>-doped ZnO obtained a higher ZT than that of  $\alpha$ -Al<sub>2</sub>O<sub>3</sub>-doped ZnO with the same preparation condition lower than 1273K.
- The differences in microstructure and thermoelectric properties with  $\alpha$ -/ $\gamma$ -Al<sub>2</sub>O<sub>3</sub>-doped ZnO can be correlated to the solid state reaction kinetics of ZnAl<sub>2</sub>O<sub>4</sub> formation.
- A possible mechanism of ZnAl<sub>2</sub>O<sub>4</sub> formation was proposed.